Supplement of Atmos. Chem. Phys., 22, 1601–1613, 2022
https://doi.org/10.5194/acp-22-1601-2022-supplement

Atmospheric Chemistry and Physics
Open Access

Supplement of

Marine gas-phase sulfur emissions during an induced phytoplankton bloom

Delaney B. Kilgour et al.

Correspondence to: Timothy H. Bertram (timothy.bertram@wisc.edu)

S1 SIO Wave Channel

Seawater used in the wave channel was pumped from below the Ellen Browning Scripps Memorial Pier in La Jolla, CA (32-52'00" N, 117-15'21" W) between 08:00 and 13:00 PST on July 23, 2019. The seawater intake was located 300 m offshore and 2 m above the ocean floor. Large pieces of organisms, such as seaweeds, were filtered out prior to the water being stored in a gravity flume on the pier. Water from the gravity flume was pumped (Grundfos UNILIFT AP12.40.04.A1) through a fire hose and a 100-micron nitex nylon mesh (Flystuff; Cat# 57-103) to remove bulk sediment before being transported in 300 gallon tanks to the SIO wave channel five minutes away. Prior to being pumped into the wave channel, the water was filtered again using a 50-micron nitex nylon mesh (Flystuff; Cat# 57-106) to prevent zooplankton from entering the wave channel. This process was continued until the glass-walled wave channel (33 m length x 0.5 m width x 1 m height) was filled with approximately 13,000 L of seawater. To simulate the wave-breaking mechanism of the ocean, waves were generated by a paddle and forced to break over an inclined ramp in the channel, simulating a beach (Prather et al., 2013; Wang et al., 2015).

S2 Mesocosm Experiment Nutrient Additions and Perturbations

A record of nutrient additions and changes that affected the wave channel seawater and bloom progression are outlined in Table S1 below. "f Medium" nutrient additions, diluted by 2 (f/2) or 20 (f/20) from the original formulation were added to stimulate algae growth (Guillard and Ryther, 1962). The phytoplankton tows and outdoor tank addition added healthy phytoplankton biomass grown under natural sunlight to increase the likelihood a bloom occurred.

S3 Dissolved DMSP and DMS Measurements

S3.1 Sample Preparation

For waterside DMSP and DMS measurements, sample preparation and cryogenic purge and trap methods closely followed Wurl (2009). All tubing, syringes, and containers were rigorously cleaned daily with 0.1% HCl, ethanol, propanol, and Milli-Q (Millipore) water for sample and standard preparation. Samples of seawater for DMSP and DMS analysis were gathered from the wave channel by siphoning seawater ~5 cm below the water surface through ¼" ID PTFE tubing into a 250 mL PTFE media bottle which was filled to overflow before closure. For $DMSP_p$ analysis, labeled as sample 1 in Equations 1-3, a ~0.1 g pellet of high-purity NaOH (Sigma Aldrich) was added directly to 5 mL of unfiltered seawater in a 15 mL headspace vial which was then immediately crimp capped with a PTFE septum. For $DMSP_d$, labeled as sample 2, a 5 mL seawater aliquot was gently syringe filtered using a 0.7 µm Whatman syringe filter into a 15 mL headspace vial after which a ~0.1 g pellet of NaOH was added before sealing. For DMS analysis, labeled as sample 3, seawater was syringe filtered (0.7 µm) and analyzed less than an hour after collection. Both $DMSP_d$ and $DMSP_p$ vials were left to rest overnight in a dark location to allow cleavage of DMSP to DMS before purge and trap analysis the following day. External standards of dissolved DMS (Sigma Aldrich) were freshly prepared and analyzed daily ranging from 0.1 to 5 nM. For samples of DMSP which exceeded the external

calibration, replicate samples were used to prepare dilutions in the calibration range. A sample CI-TOFMS chromatogram of dissolved organosulfur compounds and the external DMS calibration are in Fig. S2.

S3.2 Cryogenic Purge and Trap

Two 22 gauge needles were used to pierce the headspace vial septa with one needle positioned at the bottom of the vial and the second in the vial headspace. At a defined start time, headspace vials were bubbled with 80 sccm UHP helium (Praxair) regulated by mass flow controller (MKS) for 4 minutes. Purged gases leaving through the second needle into PTFE tubing were directed through a Nafion drier (MD-050) to remove water vapor and then passed through a Teflon loop immersed in liquid nitrogen. At the end of the purging cycle, a 6 port valve (Vici - 6UWE) was switched and the trapping loop was removed from the dewar. A carrier flow of 20 sccm helium then passed through the trapping loop, eluting the trapped gases to the analyzer inlet as the loop equilibrated to room temperature. Elution gases were diluted by 2.0 slpm N_2 before analysis.

S3.3 Chemical Ionization Time-of-Flight Mass Spectrometry (CI-TOFMS) of Dissolved Sulfur Compounds

Eluted gases were measured on a chemical ionization time-of-flight mass spectrometer using benzene cluster cation ionization which has been detailed previously (Lavi et al., 2018; Kim et al., 2016). Briefly, ~300 ppm benzene vapor was generated by passing 10 sccm N_2 vapor over a cylinder of liquid benzene and diluted with excess nitrogen to 1.9 slpm. Benzene vapor was then passed through a 20mCi Po-210 alpha source which generates benzene cluster cations. Two inline critical orifices (O'Keefe) controlled flow of benzene cluster cation vapor and analyte gases which were drawn at 1.8 slpm into an ion molecule reactor (IMR) which was held at 60 Torr, 50 V, and 50 °C. Resultant ions were directed into an electrodynamic ion funnel which focuses and gently declusters the ion beam into a RF-only transfer quadrupole before detection by a lower resolving power ($m/\Delta m \approx 1200$) time-of-flight mass spectrometer operating at 10 Hz. Peak area for m/Q 62 $[C_2H_6S]^+$ was analyzed in the Tofware graphic user interface for Igor Pro 7. Calculation of concentrations of $DMSP_p$ and $DMSP_d$ were as follows using the m/z 62 ion peak area from each sample:

$$[DMSP_p] = Sample\ 1 - Sample\ 2 - Sample\ 3 \quad (1)$$

$$[DMSP_d] = Sample\ 2 - Sample\ 3 \quad (2)$$

$$[DMS] = Sample\ 3 \quad (3)$$

S4 Bacterial Abundance and Production Measurements and Phytoplankton Enumeration

Samples for bacterial abundance (1.0 mL) were fixed with electron microscopy grade glutaraldehyde (5% v/v) and stored at -80°C after being stored at 4°C for 15 minutes and flash frozen in liquid nitrogen. Counts were performed on a FACSCanto II flow cytometer (Becton Dickinson) after SYBRGreen I staining according to Gasol and Del Giorgio (2000).

Bacterial productivity was measured by [H^3]-leucine incorporation (Kirchman et al., 1985) modified for microcentrifugation (Azam and Smith, 1992). Triplicate 1.7 mL aliquots were incubated with [H^3]-leucine (20 nM final concentration) for 1 hour. Samples with 100% trichloroacetic acid added prior to [H^3]-leucine addition served as blanks. Leucine incorporation was converted to carbon production assuming 3.1 kg C (mol leucine)$^{-1}$ (Simon and Azam, 1989).

The range of bacterial sulfur demand was estimated from bacterial productivity using the cellular C:S ratios of 86 (Fagerbakke et al., 1996) and 248 as a range (Cuhel et al., 1982). Bacterial carbon demand was estimated considering an average bacterial growth efficiency of 0.3 (del Giorgio and Cole, 1998).

Phytoplankton functional groups were enumerated by allowing 50 mL of collected seawater to settle into a settlement chamber using the Utermöhl method (Edler and Elbrächter, 2010) and analyzed with an Olympus IX-71 inverted microscope.

S5 DMS:MeSH Correlation with Salinity

It has been shown previously that DMS:MeSH may be controlled by seawater salinity (Salgado et al., 2014; Magalhães et al., 2012). Controlled experiments in which salt and DMSP were added to water samples and headspace gases were measured with gas chromatography, showed more DMS accumulated at low salinities and more MeSH accumulated at high salinities. The authors hypothesized that more DMSP is stored in cells at high salinity, causing the DMSP demethylation/demethiolation pathway to be favored over the DMSP cleavage pathway (Magalhães et al., 2012; Salgado et al., 2014). This suggests that DMS:MeSH should be inversely correlated with salinity.

Figure 5 shows a strong inverse correlation ($R^2 = 0.72$) between DMS:MeSH and salinity measurements that roughly follows linearly with days of the bloom. The salinity decline during the bloom is primarily due to the additions of ultrapure water to the wave channel meant to maintain the water level and outweigh the influence of evaporation. The change in salinity and DMSP concentrations over the 21-day bloom (1 psu; <150 nM) were significantly smaller than the salinity range and DMSP concentrations tested in controlled experiments reported in the literature (30 psu; <500 µM) (Salgado et al., 2014). A plot of DMS:MeSH as a function of salinity based on data in Salgado et al. (2014) showed the largest rate of change occurred below 15 psu salinity for these experiments, lower values than observed in the wave channel. Further, the small change in salinity observed in the wave channel is within the natural fluctuations off of Scripps Pier in summer months (Automated Shore Stations, 2021). As a result, we hypothesize that the observed correlation between DMS:MeSH and salinity during SeaSCAPE is simply a correlation and not indicative of a causal relationship between salinity and DMS:MeSH.

Table S1: Record of changes in the wave channel.

Day	Action
7/23/2019 08:00-13:00 (Day 0)	*Flume fill*
7/25/2019 17:00 (Day 2.2)	*Nutrient addition* – f/20 growth media and f/40 sodium metasilicate
7/26/2019 17:47 (Day 3.2)	*Nutrient addition* – additional silicates to bring up to f/20 sodium metasilicate
7/28/2019 17:00 (Day 5.2)	*Outdoor tank* – 300 gallons of freshly collected seawater (filtered in same manner as wave channel water) were spiked with f/2 growth media and silicates. Tank was placed outside in partial shade with a mesh screen.
8/1/2019 10:30 (Day 8.9)	*Outdoor tank addition* – Outdoor tank added to wave flume via buckets.
8/1/2019 10:45 (Day 8.9)	*Nutrient addition* – Additional growth media and silicates, to bring total concentration of both up to f/2
8/5/2019 8:15-10:30 (Day 12.8 – 12.9)	*Wall cleaning* – Removed algal growth from flume walls so that light could reach interior
8/9/2019 17:00 (Day 17.2)	*Mixing pumps* – Placed on the floor of the flume to better mix organic material
8/13/2019 17:00 (Day 21.2)	*Measurements end*

Table S2: Resolvable sulfur-containing ions in the Vocus PTR-ToF-MS mass spectrum present at signal-to-noise ratio above 3 during the campaign. Excluding DMS ($C_2H_6SH^+$), MeSH (CH_4SH^+), and benzothiazole ($C_7H_5NSH^+$), all were included in the "Other Sulfur" signal.

Ion	Exact Mass	Ion Identification	Early Bloom (Days 1-9) Mean ± 1σ (ppt)	Late Bloom (Days 10-21) Mean ± 1σ (ppt)
H_3S^+	34.995		0.11 ± 0.059	0.35 ± 0.20
CH_4SH^+	49.0107	MeSH	140. ± 44.6	98.6 ± 82.3
$C_2H_6SH^+$	63.0263	DMS	651 ± 297	$2.08 \times 10^3 \pm 1.28 \times 10^3$
$HNOSH^+$	63.9852		0.43 ± 0.19	0.84 ± 0.41
SO_2H^+	64.9692		0.21 ± 0.12	0.25 ± 0.16
$C_3H_6SH^+$	75.0263		3.9 ± 5.0	6.5 ± 4.6
$C_2H_5NSH^+$	76.0216		0.15 ± 0.45	0.25 ± 0.28
CS_2H^+	76.9514		0.10 ± 0.073	0.055 ± 0.021
CHO_2SH^+	77.977		0.19 ± 0.16	0.37 ± 0.17
$C_3H_7OS^+$	91.0212		0.63 ± 1.6	1.3 ± 2.3
$C_2H_6S_2H^+$	94.9984	DMDS	3.9 ± 3.0	9.4 ± 4.3
$C_2H_6O_2SH^+$	95.0161	$DMSO_2$	25 ± 30.	3.1 ± 8.0
$CH_5NO_2SH^+$	96.0114	MSAM	0.47 ± 0.61	0.49 ± 0.40
$C_2H_6NO_2S^+$	108.011		0.095 ± 0.19	0.22 ± 0.19
$C_5H_8NS^+$	114.037		0.70 ± 1.4	0.89 ± 1.2
$C_4H_8SO_2H^+$	121.032		56 ± 52	26 ± 17
$C_2H_6S_3H^+$	126.9704		0.090 ± 0.18	0.16 ± 0.40
$C_7H_5NSH^+$	136.0215	Benzothiazole	112 ± 67.3	146 ± 47.3
$C_7H_5NOSH^+$	152.0165	2(3H)-Benzothiazolone	0.86 ± 0.52	1.2 ± 0.15
$C_9H_{14}SH^+$	155.0889		0.73 ± 0.91	0.89 ± 1.3
$C_5H_2O_4SH^+$	158.975		0.089 ± 0.16	0.021 ± 0.037
$C_9H_{20}SH^+$	161.1358		0.16 ± 0.25	0.60 ± 0.72
$C_5H_7O_4S^+$	163.006		0.65 ± 1.0	0.72 ± 0.36
$C_7H_5NS_2H^+$	167.9936		0.72 ± 0.082	0.38 ± 0.11
$C_{10}H_{16}SH^+$	169.1045		8.3 ± 3.2	5.6 ± 0.90

$C_9H_7NOSH^+$	178.0321	2-acetyl-benzothiazole	0.79 ± 0.31	0.97 ± 0.18
$C_9H_6O_2SH^+$	179.0161		0.062 ± 0.11	0.20 ± 0.086
$C_{11}H_{16}SH^+$	181.105		7.5 ± 2.8	4.8 ± 0.97

145

150

155

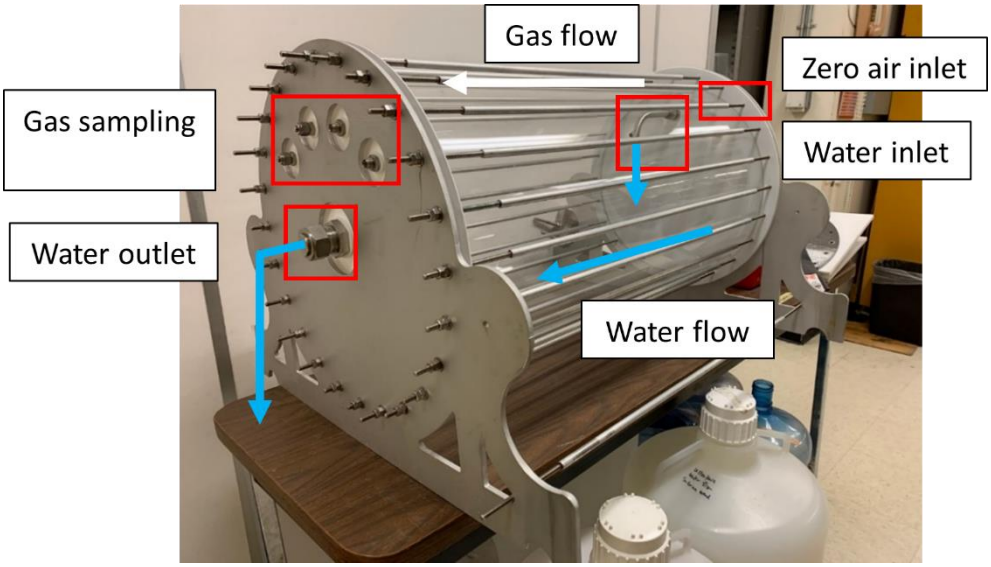

Figure S1: Picture of the isolated sampling vessel (ISV) used for gas sampling. Water enters the ISV through the water entry port after being pumped from the wave channel using a peristaltic pump and Tygon tubing. The water entry port is located on the far PTFE disk of the ISV, where the curved fitting allows for water to be introduced in a plunging jet motion. Zero air enters the ISV through a ¼" stainless steel Swagelok bulkhead fitting next to the water inlet. The near side of the ISV shows four ¼" stainless steel Swagelok bulkhead fittings arranged in a semicircle at the top of the PTFE disk. These were used for gas sampling. All gas tubing used in the experiment is ¼" O.D. PFA. Water drains back into the wave channel through the 1" water outlet port located halfway up the PTFE disk. The ISV is made of borosilicate glass with O.D., thickness, and length of 400 mm, 6 mm, and 73.66 cm respectively, leading to an ISV volume of 0.0871 m^3. In operation, the ISV was approximately half filled with water (0.0436 m^3). The zero air flow rate through the headspace was 8-10 slpm (average residence time of 5 minutes), and water flow rate was 1.5 slpm (water residence time 29 minutes).

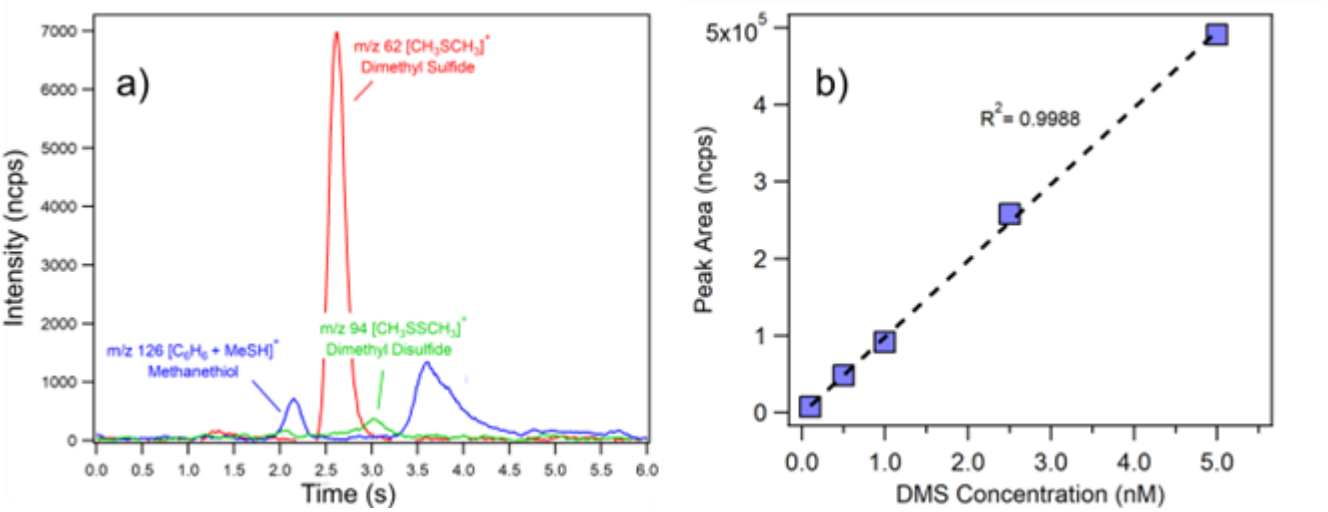

185 **Figure S2: (a) Typical cryogenic purge and trap CI-TOFMS chromatogram of SeaSCAPE seawater featuring multiple organosulfur peaks. (b) Example daily DMS external calibration of cryogenic purge and trap CI-TOFMS.**

190

195

200

205

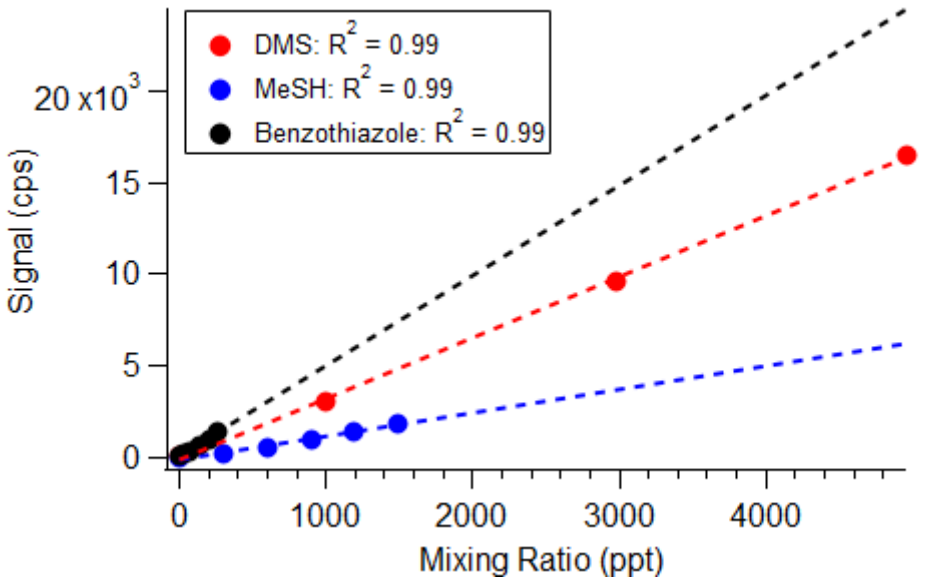

Figure S3: Example calibration curves for DMS, MeSH, and benzothiazole diluted in dry zero air. Average dry sensitivities for DMS, MeSH, and benzothiazole are 3.0, 1.0, and 5.8 cps ppt^{-1}, respectively.

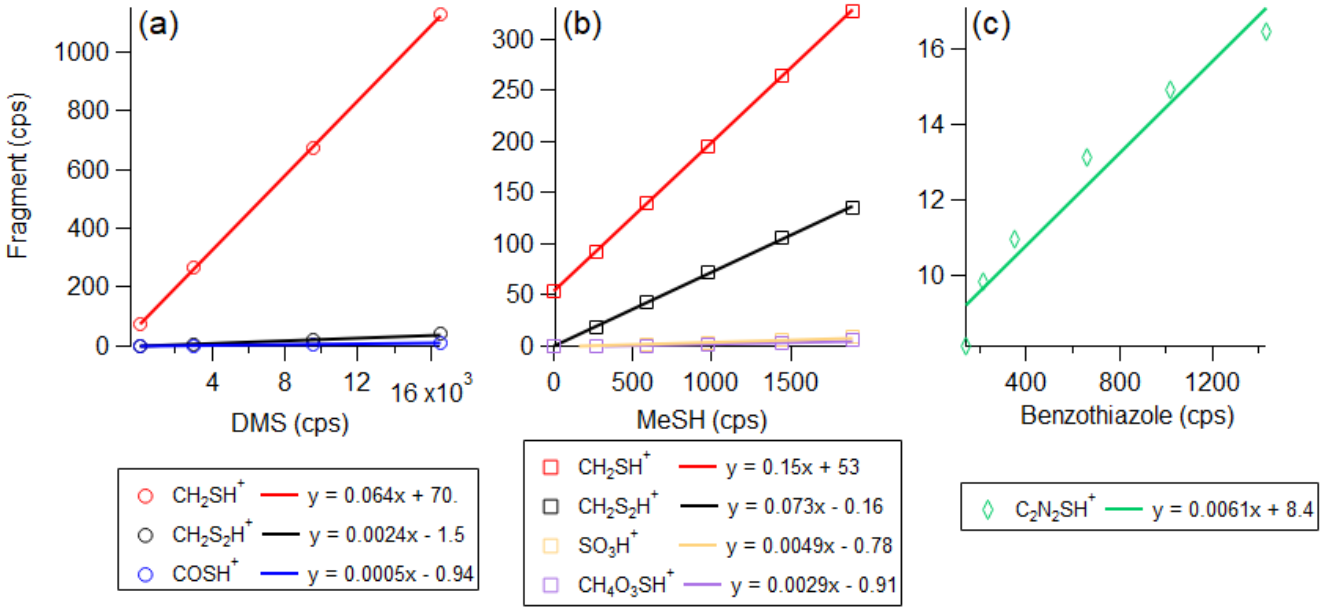

Figure S4: (a) DMS, (b) MeSH, and (c) benzothiazole fragments present in calibrations are displayed. The fragment ions are not included in the "Other Sulfur" ions, as they are not unique molecules.

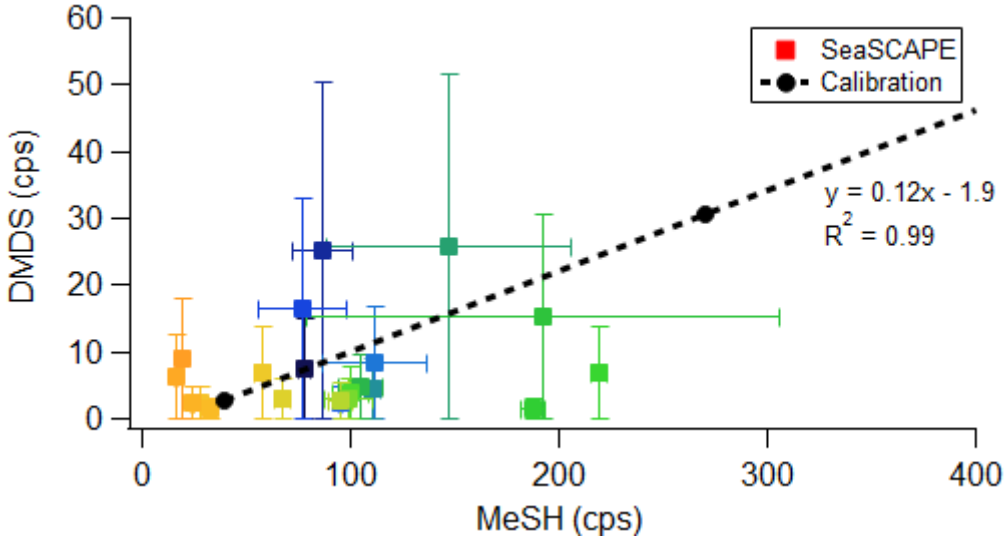

Figure S5: There exists no correlation between MeSH and DMDS during SeaSCAPE, despite a small dependence of DMDS on MeSH during post-SeaSCAPE calibrations.

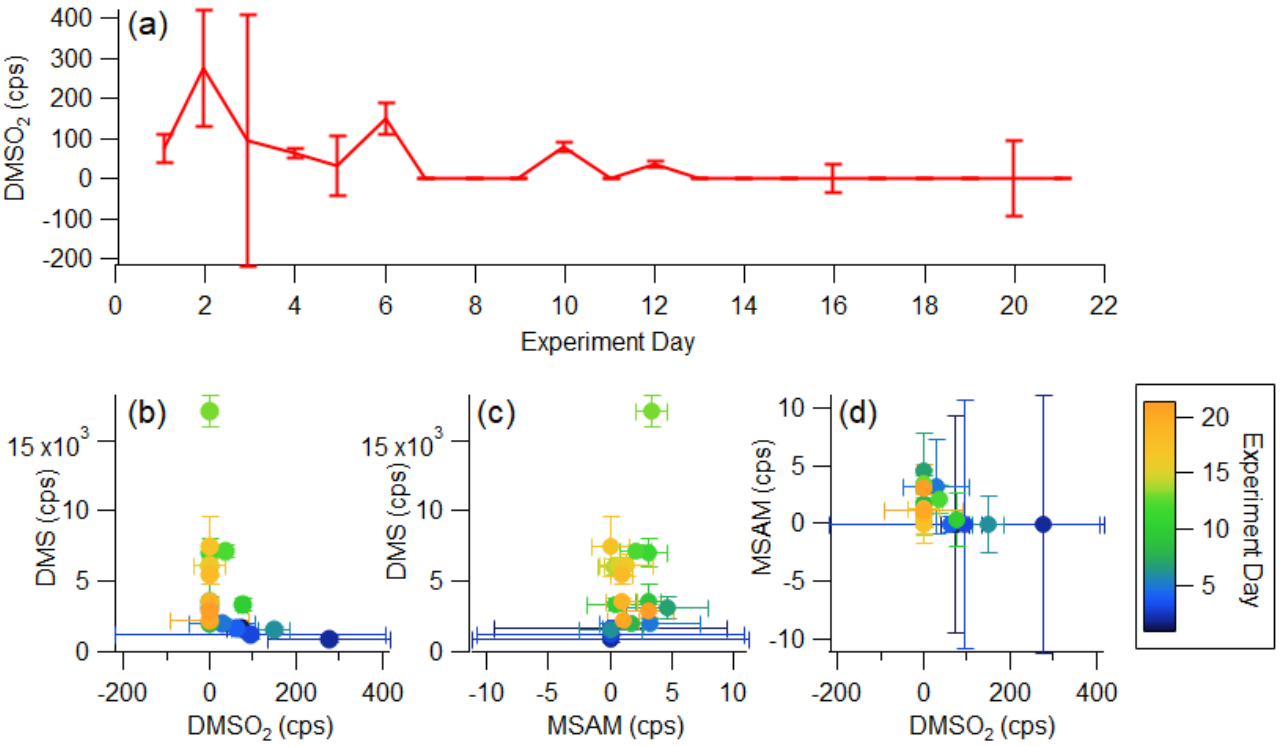

Figure S6: (a) Time series of $DMSO_2$. Correlations between (b) $DMSO_2$ and (c) methane sulfonamide (MSAM) with DMS are weak and represent minor contributors to the total "Other S" signal. DMSO is not detectable above signal-to-noise ratio 3 for any day of SeaSCAPE. (d) MSAM and $DMSO_2$ are also weakly anti-correlated (r = -0.48), in contrast to what was observed in the Arabian Sea (Edtbauer et al., 2020).

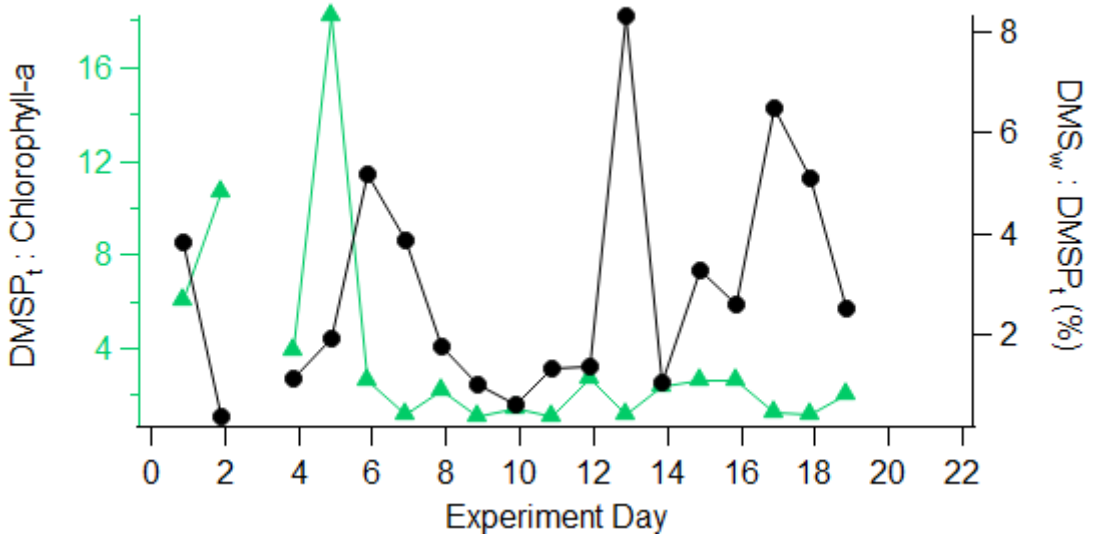

Figure S7: Time series of $DMSP_t$:chlorophyll-a, suggesting the bloom was dominated by a community of low DMSP producers, and DMS_w:$DMSP_t$, showing a low conversion efficiency of $DMSP_t$ to DMS.

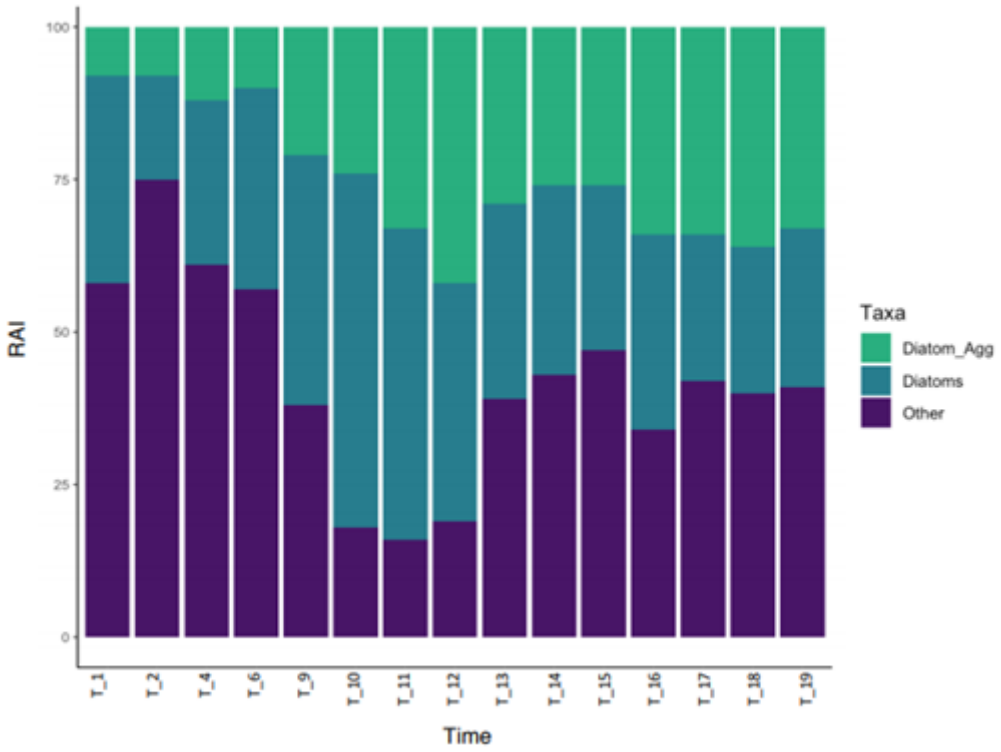

Figure S8: Time series in experiment day of the relative abundance of diatom aggregates, diatoms, and other taxa. Diatoms were dominant after day six.

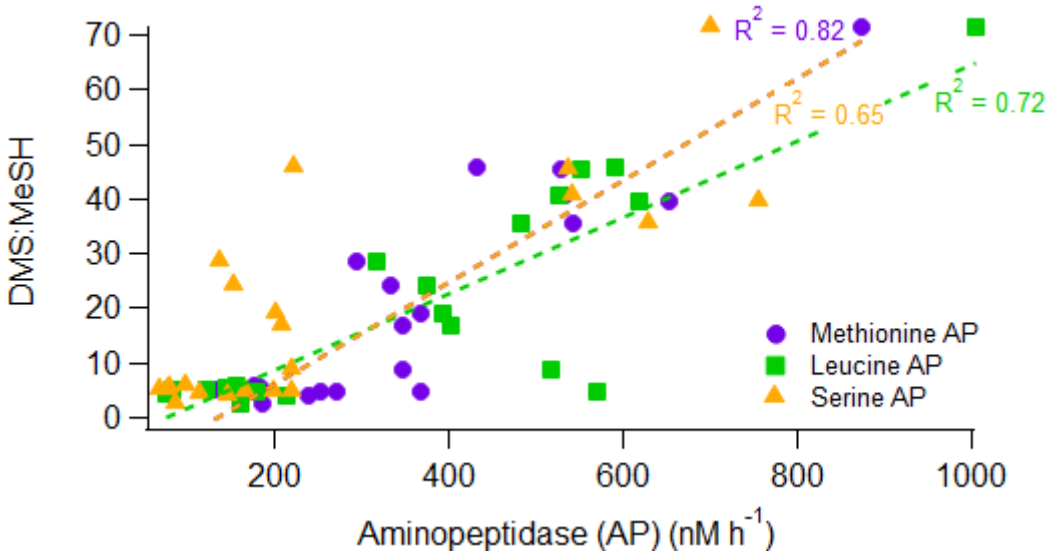

Figure S9: Regression between methionine, leucine, and serine aminopeptidase activity with DMS:MeSH, suggesting more protein degradation with higher DMS:MeSH.

References

Automated Shore Stations: https://sccoos.org/data/autoss/, last access: 19 May 2021.

Azam, F. and Smith, D. C.: A simple, economical method for measuring bacterial protein synthesis rates in seawater using 3H-leucine, Mar. Microb. Food Webs, 6, 107–114, 1992.

Cuhel, R. L., Taylor, C. D., and Jannasch, H. W.: Assimilatory Sulfur Metabolism in Marine Microorganisms: Sulfur Metabolism, Protein Synthesis, and Growth of Alteromonas luteo-violaceus and Pseudomonas halodurans During Perturbed Batch Growtht, APPL Env. MICROBIOL, 43, 9, 1982.

Edler, L. and Elbrächter, M.: The Utermöhl method for quantitative phytoplankton analysis, in: Microscopic and Molecular Methods for Quantitative Phytoplankton Analysis, 13–20, 2010.

Edtbauer, A., Stönner, C., Pfannerstill, E. Y., Berasategui, M., Walter, D., Crowley, J. N., Lelieveld, J., and Williams, J.: A new marine biogenic emission: methane sulfonamide (MSAM), DMS and DMSO measured in air over the Arabian Sea, Gases/Field Measurements/Troposphere/Chemistry (chemical composition and reactions), https://doi.org/10.5194/acp-2019-1021, 2020.

Fagerbakke, K., Heldal, M., and Norland, S.: Content of carbon, nitrogen, oxygen, sulfur and phosphorus in native aquatic and cultured bacteria, Aquat. Microb. Ecol., 10, 15–27, https://doi.org/10.3354/ame010015, 1996.

Gasol, J. M. and Del Giorgio, P. A.: Using flow cytometry for counting natural planktonic bacteria and understanding the structure of planktonic bacterial communities, Sci. Mar., 64, 197–224, https://doi.org/10.3989/scimar.2000.64n2197, 2000.

del Giorgio, P. A. and Cole, J. J.: BACTERIAL GROWTH EFFICIENCY IN NATURAL AQUATIC SYSTEMS, Annu. Rev. Ecol. Syst., 29, 503–541, https://doi.org/10.1146/annurev.ecolsys.29.1.503, 1998.

Guillard, R. R. L. and Ryther, J. H.: STUDIES OF MARINE PLANKTONIC DIATOMS: I. CYCLOTELLA NANA HUSTEDT, AND DETONULA CONFERVACEA (CLEVE) GRAN., Can. J. Microbiol., 8, 229–239, https://doi.org/10.1139/m62-029, 1962.

Kim, M. J., Zoerb, M. C., Campbell, N. R., Zimmermann, K. J., Blomquist, B. W., Huebert, B. J., and Bertram, T. H.: Revisiting benzene cluster cations for the chemical ionization of dimethyl sulfide and select volatile organic compounds, Atmospheric Meas. Tech., 9, 1473–1484, https://doi.org/10.5194/amt-9-1473-2016, 2016.

Kirchman, D., K'Nees, E., and Hodson, R.: Leucine Incorporation and Its Potential as a Measure of Protein Synthesis by Bacteria in Natural Aquatic Systemst, APPL Env. MICROBIOL, 49, 9, 1985.

Lavi, A., Vermeuel, M. P., Novak, G. A., and Bertram, T. H.: The sensitivity of benzene cluster cation chemical ionization mass spectrometry to select biogenic terpenes, Atmospheric Meas. Tech., 11, 3251–3262, https://doi.org/10.5194/amt-11-3251-2018, 2018.

Magalhães, C., Salgado, P., Kiene, R. P., and Bordalo, A. A.: Influence of salinity on dimethyl sulfide and methanethiol formation in estuarine sediments and its side effect on nitrous oxide emissions, Biogeochemistry, 110, 75–86, https://doi.org/10.1007/s10533-011-9690-z, 2012.

Prather, K. A., Bertram, T. H., Grassian, V. H., Deane, G. B., Stokes, M. D., DeMott, P. J., Aluwihare, L. I., Palenik, B. P., Azam, F., Seinfeld, J. H., Moffet, R. C., Molina, M. J., Cappa, C. D., Geiger, F. M., Roberts, G. C., Russell, L. M., Ault, A. P., Baltrusaitis, J., Collins, D. B., Corrigan, C. E., Cuadra-Rodriguez, L. A., Ebben, C. J., Forestieri, S. D., Guasco, T. L.,

Hersey, S. P., Kim, M. J., Lambert, W. F., Modini, R. L., Mui, W., Pedler, B. E., Ruppel, M. J., Ryder, O. S., Schoepp, N. G., Sullivan, R. C., and Zhao, D.: Bringing the ocean into the laboratory to probe the chemical complexity of sea spray aerosol, Proc. Natl. Acad. Sci., 110, 7550–7555, https://doi.org/10.1073/pnas.1300262110, 2013.

Salgado, P., Kiene, R., Wiebe, W., and Magalhães, C.: Salinity as a regulator of DMSP degradation in Ruegeria pomeroyi DSS-3, J. Microbiol., 52, 948–954, https://doi.org/10.1007/s12275-014-4409-1, 2014.

Simon, M. and Azam, F.: Protein content and protein synthesis rates of planktonic marine bacteria, Mar. Ecol. Prog. Ser., 51, 201–213, https://doi.org/10.3354/meps051201, 1989.

Wang, X., Sultana, C. M., Trueblood, J., Hill, T. C. J., Malfatti, F., Lee, C., Laskina, O., Moore, K. A., Beall, C. M., McCluskey, C. S., Cornwell, G. C., Zhou, Y., Cox, J. L., Pendergraft, M. A., Santander, M. V., Bertram, T. H., Cappa, C. D., Azam, F., DeMott, P. J., Grassian, V. H., and Prather, K. A.: Microbial Control of Sea Spray Aerosol Composition: A Tale of Two Blooms, ACS Cent. Sci., 1, 124–131, https://doi.org/10.1021/acscentsci.5b00148, 2015.

Wurl, O. (Ed.): Practical Guidelines for the Analysis of Seawater, CRC Press, https://doi.org/10.1201/9781420073072, 2009.